DTIC
ELECTE
JUL 27 1990
D
D&
FILE COPY
NO.10096
AD-A224 501

Reprinted from the Journal of the American Ceramic Society, Vol. 68, No. 2, February 1985
Copyright 1985 by The American Ceramic Society
J. Am. Ceram. Soc. 68 [2] 49–58 (1985)

REVIEW — Graphical Displays of the Thermodynamics of High-Temperature Gas-Solid Reactions and Their Application to Oxidation of Metals and Evaporation of Oxides

V. L. K. LOU*

General Electric Company, Research and Development Center, Schenectady, New York 12301

T. E. MITCHELL* and A. H. HEUER*

Department of Metallurgy and Materials Science, Case Institute of Technology, Case Western Reserve University, Cleveland, Ohio 44106

The construction and utility of volatility diagrams — isothermal plots showing the partial pressures of two gaseous species in equilibrium with the several condensed phases possible in a system — are demonstrated for simple oxides with reference to the Mg-O, Al-O, and Si-O systems and compared with Ellingham-type representations of these same data. Both types of diagrams are useful for providing a condensed format for a great deal of thermodynamic information. Their use is illustrated by analyzing the oxidation of Mg, Al, and Si and the volatilization of MgO, Al_2O_3, and SiO_2 in both neutral and reducing gases.

I. Introduction

THERMODYNAMIC data on many oxides, nitrides, carbides, and other high-temperature ceramics are readily available. Extensive compilations of such data are found in the Appendix of Kubaschewski's Metallurgical Thermochemistry,[1] the Metals Handbook,[2] the JANAF Tables,[3] and the Thermodynamical Properties of Inorganic Substances.[4] This information is essential for understanding high-temperature processing and high-temperature service of these ceramics, as well as the native metals from which they are made, but the data can be overwhelming. In the V-O system for example, the JANAF Tables report on the four states of vanadium metal and 10 different forms of oxides, and it is virtually impossible to use these data in practice without further calculation. Thus, when one is investigating the thermodynamics of a particular system, the question often is not whether the relevant data are available, but how to utilize the data.

Lengthy calculations can always be done on the dozen or more reactions that are possible in each system. This is not only inconvenient but often unsatisfactory, because in a complex system where many compounds exist, it is pertinent to have an overview of the relations between them, and formulae and calculations alone are generally unsatisfactory for this purpose. The best approach is often by graphical representation. The Ellingham or Richardson diagram is one example of the value of graphical representation. One single Ellingham diagram contains more information on metals and their oxides than pages of tabulated thermodynamic free energies. In fact, this diagram contains full data on the oxidation/reduction behavior of solid oxides in all types of environments and at all temperatures and has proved to be indispensable to large numbers of users. Pourbaix diagrams are of similar usefulness to corrosion scientists. As will be discussed below it is possible to extend the utility of Ellingham diagrams to include data on volatilization of oxides.

High-temperature materials engineers are often confronted with gas-solid reactions of various types — oxidation, reduction, evaporation, etc. For example, gas-solid reactions are currently of considerable interest in nitride ceramics, in that these materials are much less stable than the traditional oxide ceramics, and N_2 evolution may be unavoidable during high-temperature processing or service. For more familiar ceramics, many oxides are sintered in H_2 or CO/CO_2 environments so that reactions involving volatile sub-oxides are important. The loss of dopants at high temperatures and the contamination of ceramic wares by impurities are further examples.

The standard Ellingham-type diagram can be helpful in some cases, but alternate representations are also useful. In particular, we have found that "volatility" diagrams are appropriate for dealing with high-temperature ceramics when more than one gaseous species is involved. Volatility diagrams are isothermal plots showing the partial pressures of two gaseous species in equilibrium with the various condensed phases possible in the system. They permit ready understanding of the high-temperature chemistry and allow appropriate processing and service conditions to be specified. Wagner[5] used them in his study of the volatilization of SiO and SiO_2 and Blegan,[6] Colguhoun, Wild, Grieveson, and Jack,[7] Gulbransen and Jansson,[8,9] and Singhal[10] used them to define stable phase fields in the Si-O-N and Si-O-C systems. The intent of this paper is to promote the use of this type of construction in ceramic applications and also to explore new ways of simplifying and clarifying the existing construction method. Three new construction features to be introduced are the *isomolar line*, the *isobaric lines*, and the *constant* H_2O/H_2 *(or* CO_2/CO*) lines*. This paper is devoted to three simple oxides — MgO, Al_2O_3, and SiO_2; further papers will deal with the Si-O-N system and with ternary oxides, transition-metal oxides, and refractory metal oxides.

The new construction features and additional relevant data, in particular, the partial pressure of dominant metal vapor species, can be plotted on conventional Ellingham-type diagrams, and this graphical representation will be contrasted and compared with volatility diagrams. We also note that manipulation of the thermodynamic information we are treating can be handled by some of the

Received August 4, 1983, revised copy received May 17, 1984, approved October 17, 1984
Supported by AFOSR under Contract No. F49620-78C-0053
*Member, the American Ceramic Society

DISTRIBUTION STATEMENT A
Approved for public release
Distribution Unlimited

Table I. Reactions in Mg-O, Al-O, and Si-O Systems Needed for Plotting Volatility Diagrams

Equation No	Reaction	log K (1900 K)
1*	$2MgO(c) \rightarrow 2Mg(l) + O_2$	−21.32
2*	$Mg(l) \rightarrow Mg(g)$	1.28
3	$2MgO(c) \rightarrow 2Mg(g) + O_2$	−18.75
4*	$2Mg(l) + O_2 \rightarrow 2MgO(g)$	7.12
5	$MgO(c) \rightarrow MgO(g)$	−7.10
6	$Al_2O_3(c) \rightarrow 2Al(l) + \frac{3}{2}O_2$	−29.36
7	$Al(l) \rightarrow Al(g)$	−2.55
8	$Al_2O_3(c) \rightarrow 2Al(g) + \frac{3}{2}O_2$	−34.46
9	$4Al(l) + O_2 \rightarrow 2Al_2O(g)$	14.44
10	$Al_2O_3(c) \rightarrow Al_2O(g) + O_2$	−22.14
11	$Al_2O_3(c) + 4Al(l) \rightarrow 3Al_2O(g)$	−7.69
12	$2Al(l) + O_2 \rightarrow 2AlO(g)$	2.90
13	$2Al_2O_3(c) \rightarrow 4AlO(g) + O_2$	−52.91
14	$Al_2O_3(c) + Al(l) \rightarrow 3AlO(g)$	−25.00
15	$Al(l) + O_2 \rightarrow AlO_2(g)$	5.16
16	$2Al_2O_3(c) + O_2 \rightarrow 4AlO_2(g)$	−38.09
17	$2Al_2O_3(c) \rightarrow 3AlO_2(g) + Al(l)$	−43.25
18	$SiO_2(l) \rightarrow Si(l) + O_2$	−15.68
19	$Si(l) \rightarrow Si(g)$	−4.92
20	$SiO_2(l) \rightarrow Si(g) + O_2$	−20.60
21	$2Si(l) + O_2 \rightarrow 2SiO(g)$	13.86
22	$2SiO_2(l) \rightarrow 2SiO(g) + O_2$	−17.50
23	$SiO_2(l) + Si(l) \rightarrow 2SiO(g)$	−1.82
24	$Si(l) + O_2 \rightarrow SiO_2(g)$	8.29
25	$SiO_2(l) \rightarrow SiO_2(g)$	−7.30

*Note that 1900 K is above the boiling point of Mg.

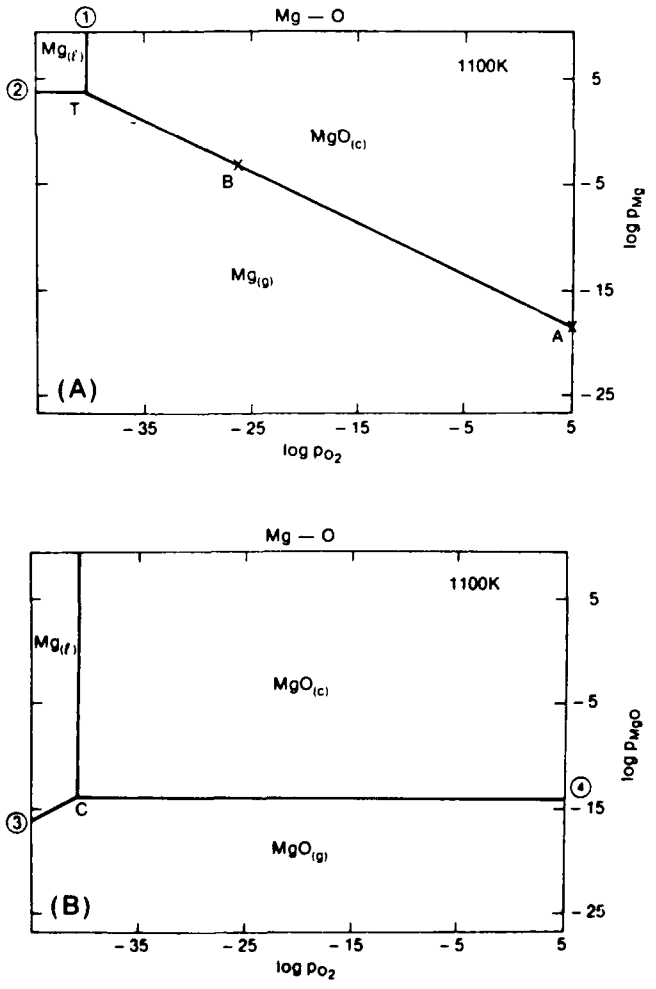

Fig. 1. (*A*) Volatility diagram for the Mg-O system at 1100 K for case when only Mg(*g*) is considered. In this and all other figures, pressures are given in Pa (1 atm = 1.013×10^5 Pa). (*B*) Volatility diagram as per (*A*) but with MgO(*g*) considered.

computer programs now extant, e.g., SOLGASMIX.[11] However, graphical techniques have some advantages and our intention in this paper is to emphasize the ease of handling these data graphically using only the JANAF Tables. Before beginning our discussion, we note that, whether a computer program or a graphical display is used, there is always the danger of missing important species. *Caveat emptor!*

II. Data Base — Gaseous and Nongaseous Phases

Three common oxide systems will be dealt with here — Mg-O, Al-O, and Si-O. The thermodynamic data appropriate for these systems are tabulated in the JANAF Tables. In the Mg-O system, they are Mg (reference state), Mg(*c*),* Mg(*l*), Mg(*g*), $Mg^+(g)$, MgO(*c*), MgO(*l*), and MgO(*g*); in the Al-O system, they are Al (reference state), Al(*c*), Al(*l*), Al(*g*), $Al^-(g)$, AlO(*g*), $AlO^-(g)$, $AlO_2(g)$, $AlO_2^-(g)$, $Al_2O(g)$, $Al_2O_2(g)$, α-$Al_2O_3(c)$, γ-$Al_2O_3(c)$, and $Al_2O_3(l)$; and in the SiO system, they are Si (reference state), Si(*c*), Si(*l*), Si(*g*), $Si_2(g)$, $Si_2(g)$, $Si_3(g)$, SiO(*g*), quartz $SiO_2(c)$, cristobalite $SiO_2(c)$, $SiO_2(l)$, and $SiO_2(g)$. For the temperature range of interest, all three metals and SiO_2 are in the liquid state, and one can reduce the condensed phases to Mg(*l*), Al(*l*), Si(*l*), MgO(*c*), α-$Al_2O_3(c)$, and $SiO_2(l)$. Furthermore one can reduce the number of gaseous species to be considered, as many of them have very low vapor pressures. Thus, one can eliminate all the charged radicals as well as dimeric and trimeric compounds for their influences are exerted by their monomeric counterparts. The gaseous phases that need to be considered are Mg(*g*), MgO(*g*), Al(*g*), AlO(*g*), $Al_2O(g)$, Si(*g*), SiO(*g*), and $SiO_2(g)$.

Even with this reduced number of species in each system, a large number of reactions have to be considered. Volatility diagrams are useful when reactions involving at least one condensed species and no more than one volatile species (except oxygen) are considered: reactions involving only gases are neglected. Table I is a tabulation of the 25 various reactions in these systems needed for the diagrams; for convenience, log K values at 1900 K are also given. All can be represented in standard thermodynamic form, i.e.

$$\Delta G = RT \ln K \qquad (K = \Pi^P a_i''^{n_i''} / \Pi^R a_i'^{n_i'})$$

where P stands for product, R for Reactant, a for activity, and n for integer.

III. Construction and Utilization of Volatility Diagrams

(1) *The Mg-O System*

(*A*) *Construction:* Volatility diagrams for oxides are always constructed with log p_{O_2} as the abscissa and log p_M or log p_{MO} as the ordinate. At 1100 K, equilibrium constants for Eqs. (1) to (5) in Table I can be either taken directly from the JANAF Tables or calculated from data given in these tables. Equation (1), which describes the oxidation of Mg to MgO, has an equilibrium constant of $10^{45.6}$ and, as it is independent of p_{Mg}, is shown in Fig. 1(*A*) as vertical line 1–*T* that separates the Mg(*l*) and MgO(*c*) phase fields. Similarly Eq. (2), the evaporation of liquid Mg, is independent of p_{O_2} and is shown as the horizontal line 2–*T*. Equation (3) describes the evaporation of MgO to form Mg(*g*) and O_2; as it involves both p_{Mg} and p_{O_2}, it is plotted in Fig. 1(*A*) as the sloping line *T*–*A* with a gradient of $-\frac{1}{2}$. The intersection of these three lines, *T*, indicates the minimum p_{O_2} needed to prevent reduction of MgO(*c*) and the maximum p_{Mg} possible in the system. At 1100 K the minimum log p_{O_2} is −40.6 (Pa) and the maximum log p_{Mg} is 3.8 (Pa). The significance of the sloping line is that p_{Mg} decreases with increasing p_{O_2}; thus, in an ambient pressure of 10^5 Pa (1 atm) of oxygen (point *A*), volatilization of MgO is unlikely because of the very low equilibrium partial pressure of Mg, 10^{-19} Pa.

Normally, weight loss due to evaporation in a high-temperature experiment is important only if the vapor pressure of the evapo-

*The suffix *c* stands for crystal, *l* for liquid, and *g* for gas

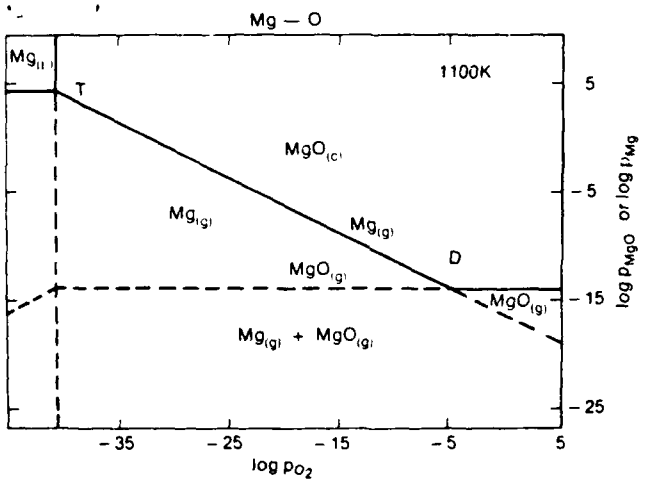

Fig. 2. Volatility diagram for the Mg-O system at 1100 K.

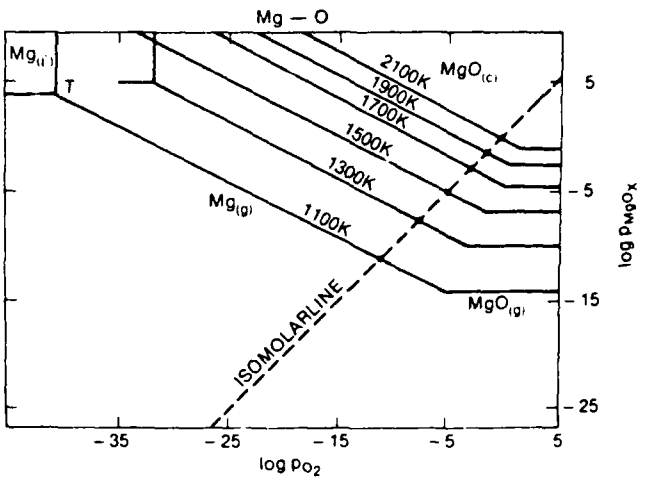

Fig. 3. Master volatility diagram for the Mg-O system from 1100 to 2100 K; isomolar line is defined in text.

rating species is higher than 10^{-4} Pa. Point B in Fig. 1(A) corresponds to this arbitrary condition, and a decrease in p_{O_2} beyond this point will result in significant weight loss.

A similar diagram can be constructed for MgO vapor by utilizing Eqs. (1), (4), and (5), as shown in Fig. 1(B) where log p_{MgO} is plotted on the ordinate instead of log p_{Mg}. Equation (4) is an alternative oxidation reaction and depends on both p_{MgO} and p_{O_2}; it is shown as the sloping line 3–C with a gradient of $+\frac{1}{2}$; Eq. (5), which describes the evaporation of MgO vapor over solid MgO, is independent of p_{O_2} and constant at 10^{-14} Pa (line C–4). The next step in the construction is to combine Figs. 1(A) and (B) into one diagram and to discard unimportant lines, as shown in Fig. 2. In the approximation we use, only the solid lines are important in this figure because the dashed lines represent species with smaller vapor pressures; we henceforth refer to these solid lines as maximum equilibrium pressure lines for obvious reasons. The intersection D, which we shall call the major vapor transition point, delineates the field where the major vapor species changes; to its right, it is MgO vapor and to its left, it is Mg vapor. It is easy to construct a number of such simple isothermal volatility diagrams which can be combined into a master diagram covering the temperature range of interest. Figure 3 is such a diagram for the Mg-O system and contains all the vital thermodynamic data on volatilization reactions between 1100 and 2100 K.

(B) Evaporation of MgO in Vacuum and Inert Gases and the Use of the Isomolar Line: When MgO(g) is the major species, i.e., at values of p_{O_2} to the right of point D, the vapor pressure of MgO in a closed system will be constant; the evaporation of MgO to MgO(g) (reaction 5) does not depend on p_{O_2}. However, if the p_{O_2} is reduced, the principal vapor species will change to Mg(g) and the vapor pressure will increase following the line T–D in Fig. 2.

However, there is one other important fact of such an experiment that must be considered, the *mass balance criterion*. When 1 mol of MgO(c) undergoes evaporation via Eq. (3), 1 mol of Mg(g) and $\frac{1}{2}$ mol of O_2 are produced. Assuming ideal gas behavior and equal diffusivity of all gaseous species, the mass balance criterion stipulates that $p_{Mg} = 2p_{O_2}$ or log p_{Mg} = log p_{O_2} + log 2. This relation is shown in Fig. 3 as the dashed line. We henceforth refer to it as an *isomolar line* and its gradient is always 1. At the point of intersection of the isomolar line with a maximum equilibrium pressure line, both the mass balance criterion and the thermochemistry are satisfied. The predicted equilibrium vapor pressures above crystalline MgO at 1900 K, for example, are p_{Mg} = 0.1 Pa and p_{O_2} = 0.05 Pa. Other isomolar points are also indicated by filled circles. Conceptually, when an MgO crystal dissociates into Mg vapor and O_2, the respective partial pressures are controlled in a fixed ratio by the equilibrium constant. The isomolar line defines the maximum p_{Mg} over MgO(c) in a nonreactive environment and sets a limit to the valid portion of the volatility diagram; only conditions to the right of this line are attainable.

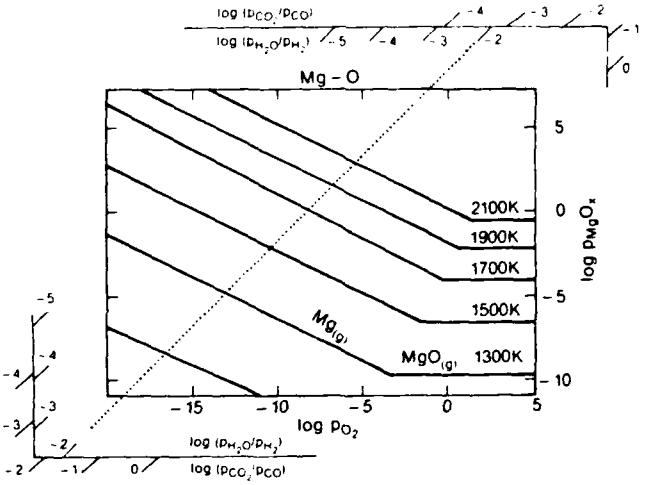

Fig. 4. Volatility diagram for Mg-O system with H_2O/H_2 and CO_2/CO nomographs included.

(C) Evaporation of MgO in Reducing Gases and the Use of the Isobaric Lines: It is well-known that reducing gases can cause severe weight loss of MgO at high temperatures; volatility diagrams can predict the vapor pressures of various gaseous species involved in the high-temperature reactions. In fact the isomolar point at any particular temperature is no longer applicable as the Mg vapor pressure is much higher with a reactive gas. For example, in the case of hydrogen with an H_2O to H_2 ratio of 10^{-2}, the JANAF Tables predict that log p_{O_2} at 1900 K will be −6.7 (Pa), and according to Fig. 3 the corresponding log p_{Mg} is 1.5 (Pa). The calculation can be repeated for other temperatures, and the argument presented in the Appendix shows that for a specific H_2O to H_2 ratio, the equilibrium p_{O_2} and p_{Mg} for various temperatures fall on a single straight line; the dotted line in Fig. 4 is constructed for an H_2O to H_2 ratio of 10^{-2}. As can be seen in this figure, a nomographic-type construction is possible: a straight edge can be placed on any desired H_2O to H_2 (or CO_2 to CO) ratio so that the equilibrium p_{O_2} above MgO can be determined at any temperature. The effect of moisture in the ambient is easily predicted from Fig. 4. At 1900 K, for example, if the H_2O to H_2 ratio changes from 10^{-2} to 10^{-1}, log p_{Mg} increases from 1.5 to 2.5 (Pa) and the

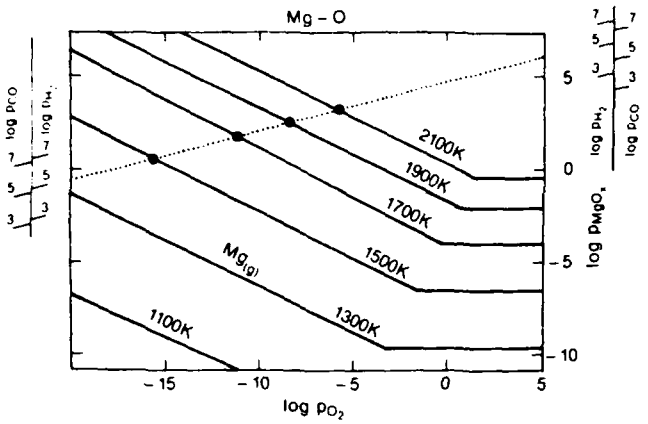

Fig. 5. Volatility diagram for the Mg-O system with isobaric line (dotted) included.

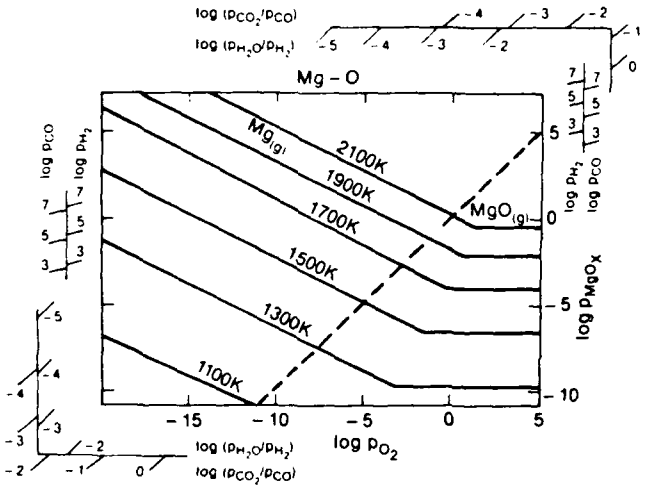

Fig. 6. Complete volatility diagram for the Mg-O system.

evaporation rate should likewise increase.

At first sight, p_{Mg} can increase up to the point T where Mg(l) and MgO(c) are in equilibrium with MgO(g). However, such a direct interpretation of the volatility diagram must be modified to take cognizance of the mass balance. The reaction between MgO and H_2 is

$$MgO(c) + H_2(g) \rightarrow Mg(g) + H_2O(g)$$

and using the same assumption we made earlier, for every mole of Mg vapor produced, 1 mol of H_2O vapor is also produced. As in the case of the nonreactive environment, the volatilization reaction creates its own environment. One can calculate the equilibrium p_{Mg} and p_{H_2O} for this reaction by making the simple assumption that $p_{Mg} = p_{H_2O}$. At 1900 K in 10^5 Pa of dry H_2, for example, the vapor pressure of H_2O or Mg is $10^{2.2}$ Pa. We refer to this point as the *isobaric point;* it is shown in Fig. 5 as a filled circle and indicates the maximum Mg vapor pressure allowed for any p_{H_2} at one particular temperature.

The Appendix also shows that the isobaric points at constant p_{H_2} and various temperatures should fall on a straight line, the *isobaric line*, as can be seen in Fig. 5. In fact, as shown in this figure, the best way of representation is to include additional scales on the ordinates, i.e., to create another nomograph; the position of an isobaric point can be determined by placing a straightedge across the diagram for the particular H_2 pressure of interest. The effect of CO can be determined on a similar basis by using the corresponding CO scales, which are derived from the reaction

$$CO(g) + \tfrac{1}{2}O_2(g) \rightarrow CO_2(g)$$

Thus, the final volatility diagram for MgO is shown in Fig. 6. The range of validity of the diagram for nonreactive ambients is to the right of the isomolar line. For reducing environments, H_2/H_2O or CO/CO_2, the CO or H_2 nomograph is used for any particular pressure to define the validity of the volatility diagram — for any temperature, to the right of the intersection of a straight line connecting the CO or H_2 scales and the maximum equilibrium pressure line. For a given H_2O to H_2 or CO_2 to CO ratio, the appropriate scales are used to determine the equilibrium pressure on the maximum equilibrium pressure line. It is clear that all available thermodynamic information has been included in Fig. 6 in a compact and useful form.

Two additional points concerning the nomographic construction should be noted. Firstly, there is the question of volatile hydroxides and in this case $Mg(OH)_2(g)$ is the most volatile (OH)-containing species. However, our calculations based on values tabulated in the JANAF Tables suggest that it is a minor species under normal pressures and H_2O to H_2 ratios of less than 10^{-2}. Therefore, in Fig. 6, the highest log H_2O/H_2 value on the scale is -2. Actually, this is not a particularly severe limitation. A p_{H_2O} to p_H ratio of 10^{-2} corresponds to a dew point of +7°C, and $Mg(OH)_2$ formation therefore requires injection of steam into the system. Under conditions where $Mg(OH)_2$ does form, a completely different type of volatility diagram is required. Normally hydroxides are important only at high p_{H_2O} and low temperature.

With regard to the CO_2/CO scale, the limitation here is sooting of carbon, and the condition for that in the present temperature range is a CO_2 to CO ratio of about 10^{-4}. Again this is reflected in Fig. 6, where the minimum value on the log CO_2/CO scale is -4.

(D) Use of Ellingham-Type Diagrams: A useful alternative to the volatility diagram is to plot the data on the standard Ellingham-type diagram.[1] Clearly, either form will suffice since volatility diagrams are plots of equilibrium p_{O_2} vs equilibrium p_{MO_x} for various temperatures, while the Ellingham-type diagrams have equilibrium p_{O_2} and T as the abscissa and ordinate, respectively, for various p_{MO_x} values. Such a diagram for the Mg-O system is constructed in Fig. 7, where in accord with standard practice, the temperature is given in °C rather than K and the abscissa is actually $RT \ln p_{O_2}$. The nomographic constructions for p_{O_2}, H_2O to H_2 ratio, and CO_2 to CO ratio scales are well-known and will not be discussed. The data usually included in the Ellingham diagram define the oxidation of Mg to solid MgO, which are plotted as lines 1 and 3. The former represents the oxidation of solid or liquid Mg and the latter the oxidation of 10^5 Pa of Mg vapor; M is the melting point of Mg. Solid MgO is stable only above these lines, and the intersection of the two lines, B, is the boiling point of Mg. The vapor pressure of Mg over condensed Mg (Eq. (2)) at various temperatures is shown as a series of vertical lines (below line 1); lines corresponding to $>10^5$ Pa Mg pressure are not drawn. The vapor pressure of Mg over solid MgO plots as a series of sloping lines which are appropriately labeled in Fig. 7. Finally, the vaporization of MgO via Eq. (5) is shown as a series of vertical lines at the top of the diagram, line 4 corresponding to $p_{Mg} = 10$ Pa. Line 5 is the locus of the points marked D on Fig. 2 and denotes, for a given p_{Mg}, the p_{O_2}/T conditions where the major vapor species changes from Mg vapor (below the line) to MgO vapor (above the line).

At any p_{O_2}, the relevant p_{Mg} or p_{MgO} pressure can be obtained by noting which isobar passes through the intersection of the line between that p_{O_2} and point O on the left-hand vernier of the nomograph at a given T. (For example, p_{Mg} is 10 Pa at 1800°C at $p_{O_2} = 10^{-2.5}$ Pa.) In any H_2O/H_2 (or CO_2/CO) mixture, a straightedge is placed between H (or C) on the vernier and the relevant gas mixture and likewise gives the p_{MgO}, pressure as a function of temperature.

As in the volatility diagram, the valid regions of the Ellingham diagram can be determined using the mass balance criterion. In

[1]This was pointed out by a reviewer of an earlier version of this paper.

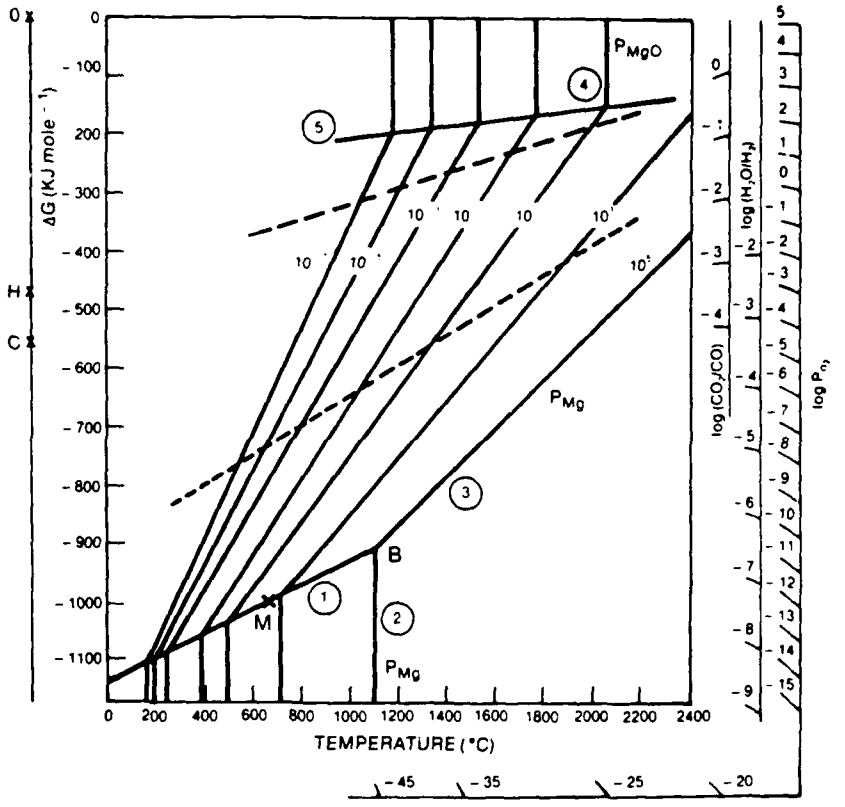

Fig. 7. Ellingham-type diagram for the Mg-O system.

vacuum or inert gases, p_{Mg} has to be equal to or less than $2p_{O_2}$ and such a condition is shown by the long-dashed isomolar line; the diagram is only valid above this line. In practice, for a given temperature, say 2000°C, the maximum Mg vapor pressure is found by noting which isobar intersects the point where the isomolar line crosses 2000°C; in addition, placing a straightedge through this point and point *O* on the vernier yields the minimum p_{O_2} as $10^{0.5}$ Pa.

The isobaric lines are constructed in a similar way, by noting that the limiting condition is $p_{Mg} < p_{H_2O}$. At 10^5 Pa H_2, for example, the isobaric line is constructed (the short-dashed line in Fig. 7) by noting the temperature at which a straight line between the *H* vernier and a series of H_2O to H_2 ratios intersects the appropriate p_{Mg} isobar; the isobaric point for $p_{H_2O} = 10^5$ Pa is at 1900°C; for 10 Pa it is 1350°C; for 10^{-1} Pa it is 1050°C, etc. The diagram is only valid above the short-dashed line in such an atmosphere.

(2) The Al-O System

(A) Construction: The JANAF Tables list 15 metallic and oxide phases in this system, of which six are relevant to the present discussion — Al(*l*), α-Al_2O_3(*c*), Al(*g*), Al_2O(*g*), AlO(*g*), and AlO_2(*g*). The 1900 K isothermal section is chosen to demonstrate the construction. The vertical line in Fig. 8 represents the oxidation of Al(*l*) to α-Al_2O_3 (Eq. (6) in Table I) and the logarithmic value of the equilibrium constant is −29.4, from which log p_{O_2} is deduced to be −14.6 (Pa). The four lines to the left of this vertical line represent the vapor pressures of the four vapor species over metallic aluminum, namely Al(*g*), Al_2O(*g*), AlO(*g*), and AlO_2(*g*), corresponding to the chemical reactions described by Eqs. (7), (9), (12), and (15). The gradients of these lines can be determined from the ratio between oxygen and the volatile species, such that for Eq. (7) it is 0, for Eq. (9) it is ½, for Eq. (12) it is ½, and for Eq. (15) it is 1. To the right of the vertical line, the four lines represent vapor pressures of the same four species over α-Al_2O_3 and the corresponding reactions are described by Eqs. (8), (10), (13), and (16), for which the corresponding gradients are −¼, −1, −¼, and ¼. For each volatile species, the lines intersect on the vertical line to form a "triple" point where Al(*l*) and Al_2O_3(*c*) are in equilibrium with a gaseous species;

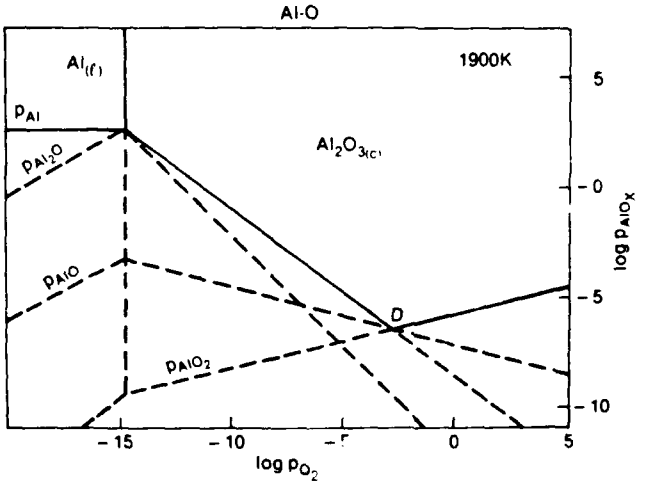

Fig. 8. Volatility diagram for the Al-O system at 1900 K.

in cases where the gases are more reduced than Al_2O_3, i.e., Al(*g*), Al_2O(*g*), and AlO(*g*), the triple points indicate the maximum possible vapor pressure of these gaseous species. These can be calculated according to Eqs. (7), (11), and (14), and their logarithmic values are 3.4, 3.4, and −3.3 (Pa). For AlO_2(*g*), which is more oxidized than Al_2O_3, the triple point does not represent the maximum vapor pressure, as it continues to increase in the oxide phase field (the reaction at this triple point is Eq. (17)). For practical purposes, the important lines in this diagram are the solid lines which show the vapor pressures of the most volatile species. It is apparent that under the most reducing conditions, the major vapor species is Al vapor but under more oxidizing conditions, i.e., to the right of *D* in Fig. 8, it is AlO_2(*g*). By use of this simplified construction, the 1700 and 2100 K sections are added in Fig. 9.

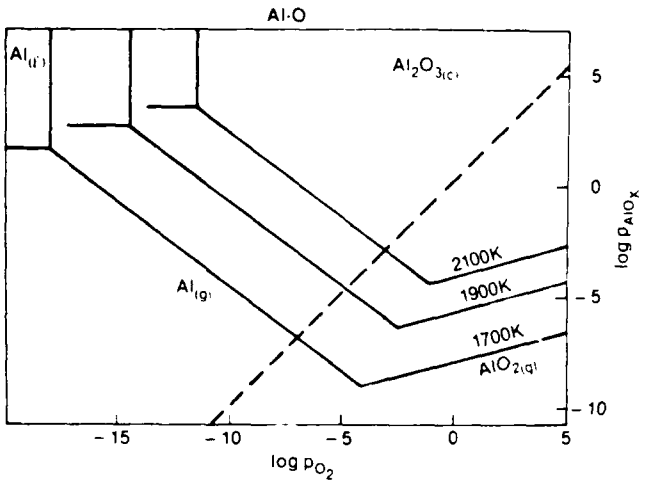

Fig. 9. Master volatility diagram for the Al-O system from 1700 to 2100 K.

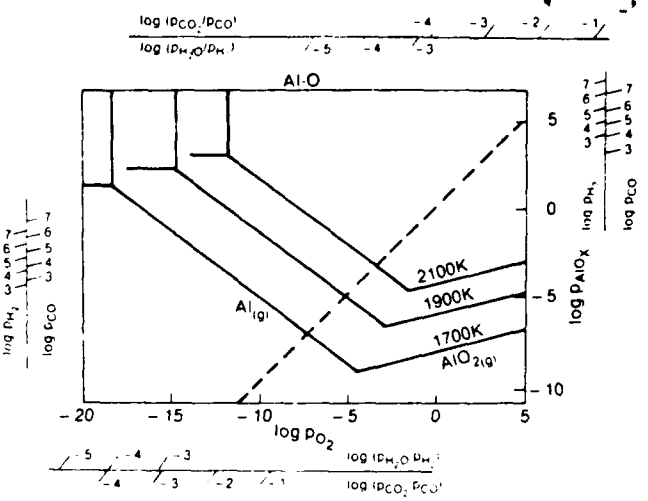

Fig. 10. Complete volatility diagram for the Al-O system.

(B) Vacuum and Inert Gases: The next step in the construction is to put in the isomolar points by considering the decomposition reaction

$$Al_2O_3(c) \rightarrow 2Al(g) + \tfrac{3}{2}O_2(g)$$

and the corresponding isomolar lines (log p_{O_2} = log ¾ + log p_{Al}— the dashed line in Fig. 9). From the intersections one can predict the maximum vapor pressures of Al(g) and oxygen over α-Al_2O_3 in a nonreactive system; for example at 1900 K, log p_{Al} = −4.8 (Pa) and log p_{O_2} = −5.0 (Pa). We stress again that the significance of the isomolar line is to define the valid portion of the diagram such that only the area to its right is accessible in nonreactive ambients.

(C) H_2 and CO: The nomographic construction of the isobaric lines in Fig. 10 is similar to that in the Mg-O system except that isobaric points are calculated according to the mass balance criterion $p_{H_2O} = \tfrac{1}{2}p_{Al}$ which follows from the reaction

$$Al_2O_3(c) + 3H_2 \rightarrow 2Al(g) + 3H_2O(g)$$

The intersections with the maximum equilibrium pressure lines indicate the maximum vapor pressures at various temperatures; for example, at 10^5 Pa of dry hydrogen at 1900 K, log p_{Al} cannot exceed 0.3 (Pa). As with the Mg-O diagram, the CO scale is also included in the diagram. The constant H_2O/H_2 and CO_2/CO lines are likewise included and p_{Al} under various ratios of these gases can be readily determined. The range of these scales are again limited by reasons explained previously; for the H_2O/H_2 scale, the upper limit is 10^{-3} (dew point of −20°C) and for the CO_2/CO scale

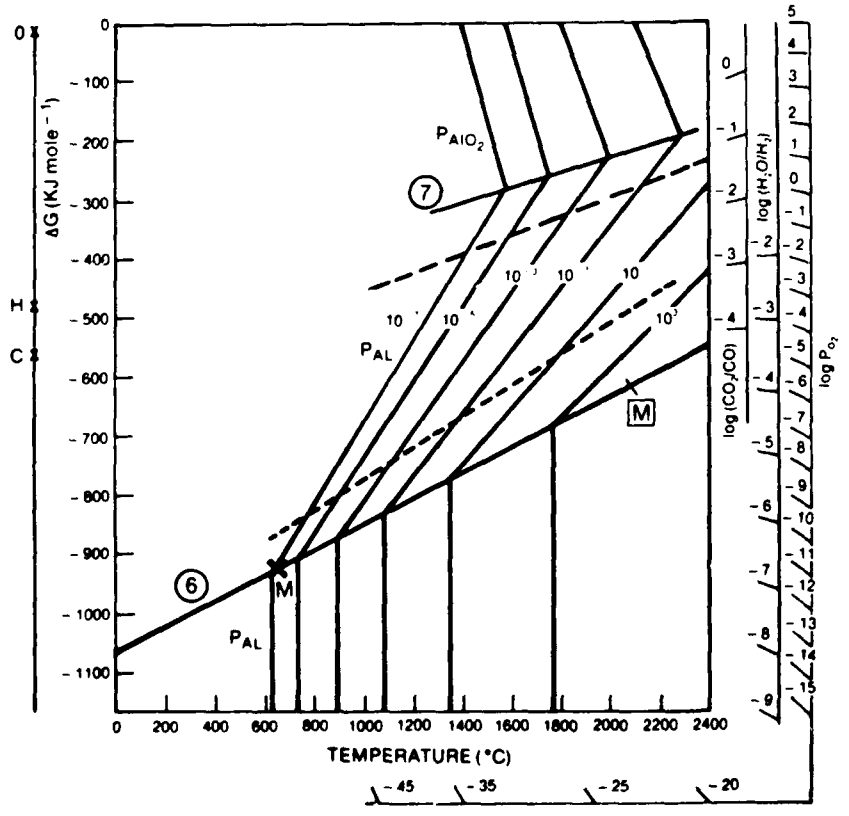

Fig. 11. Ellingham-type diagram for the Al-O system.

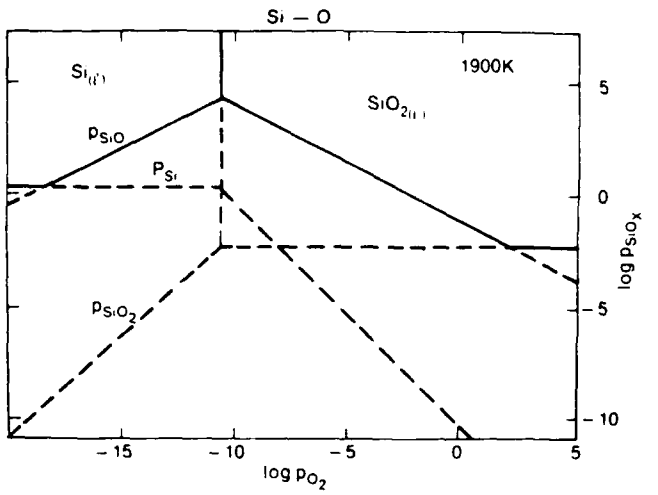

Fig. 12. Volatility diagram for the Si-O system at 1900 K.

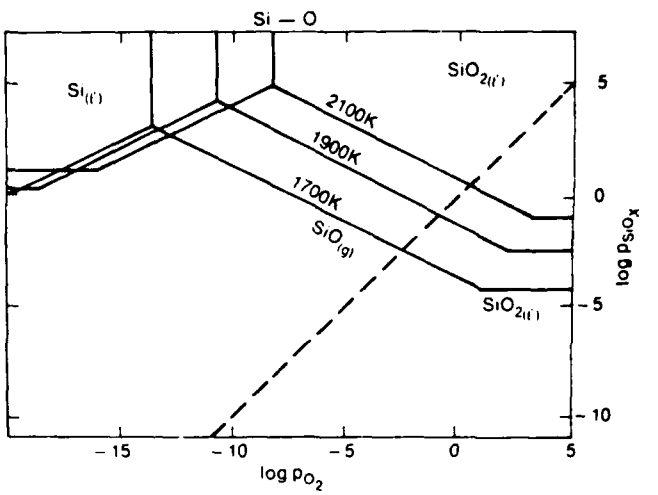

Fig. 13. Master volatility diagram for the Si-O system from 1700 to 2100 K.

the lower limit is 10^{-4}. It should again be cautioned that the region of validity for any H_2 or CO pressure is to the right of the corresponding isobaric line.

(D) Ellingham Diagram: The Ellingham-type compilation of the thermodynamic data for the Al-O system is shown in Fig. 11 and differs from Fig. 7 mainly in the vapor species found at high p_{O_2}'s; the constant $p_{Al:O_2}$ lines slope to the left and the transition from p_{Al} to p_{AlO_2} as the principal vapor species is shown as the line marked 7. Line 6 delineates the transition from Al (solid or liquid) to Al_2O_3 (solid or liquid) as the condensed phase, with M and $\boxed{M}$ being the conventional symbols for the melting points of the metal and oxide, respectively.

(3) The Si-O System

(A) Construction of the Diagram: The important phases in this system are $Si(l)$, $SiO_2(l)$, $Si(g)$, $SiO(g)$, and $SiO_2(g)$. By use of values listed in the JANAF Tables, the 1900 K volatility diagram is shown in Fig. 12. The vertical line represents the oxidation of Si to SiO_2 (Eq. (18)), the three lines to its left describe the vapor pressures of $Si(g)$, $SiO(g)$, and $SiO_2(g)$ over $Si(l)$, according to Eqs. (19), (21), and (24), respectively, and the three lines to its right describe the vapor pressures over $SiO_2(l)$, according to Eqs. (20), (22), and (25). The most volatile species is $SiO(g)$, whereas $Si(g)$ and $SiO_2(g)$ are relatively unimportant except at low and high p_{O_2}, respectively, where they become the major vapor species.

The rest of the construction is identical with the previous two systems and only a brief description will be given here. Firstly, in Fig. 13, the 1700 and 2100 K isothermal sections are included and the isomolar line, which satisfies the mass balance conditions of Eq. (22), is also drawn. As before, this line delineates the valid region of the diagram when the system is under a nonreactive environment. In hydrogen, Fig. 14 is drawn to accommodate the mass balance corresponding to the SiO_2-H_2 reactions: $SiO_2(l) + H_2 \rightarrow SiO(g) + H_2O(g)$. The maximum $SiO(g)$ vapor pressure is a function of the hydrogen pressure, and for example at 1900 K and $p_{H_2} = 10^5$ Pa, log p_{SiO} cannot exceed +2.6 (Pa). Isobaric points for other temperatures and pressures can be determined from Fig. 14. The valid portion of the diagram is to the right of the corresponding isobaric line, where p_{SiO} is determined by the H_2O to H_2 ratio of the environment. Similarly, in CO_2/CO mixtures, p_{SiO} can be determined from the diagram by using the corresponding CO_2/CO scale and the valid region of this scale is defined as before.

The Ellingham-type compilation of the data is included in Fig. 15. Line 8 delineates the transition from Si to SiO_2 as the condensed phase, and lines 9 and 10 show, respectively, transitions from SiO to SiO_2 and from Si to SiO as the principal vapor species.

(B) Active Oxidation: The Si-O system is unique in that over a large range of p_{O_2}'s, the sub-oxide (SiO) is the most important species over silicon. This differs from the Mg-O and Al-O systems where the metallic vapors $Mg(g)$ and $Al(g)$ predominate at low p_{O_2}'s. As a result, active oxidation of Si by the formation of SiO is important and has been well studied.[5,8] The physical phenomenon of active oxidation involves weight loss, while passive oxidation involves weight gain as a protective oxide film grows. The active-passive transition is defined as the p_{O_2} at which further evaporation of SiO is prevented by the formation of a passive SiO_2 film. This point was first emphasized by Wagner[5]; here, we show the utility of volatility diagrams in dealing with the active-passive transition. Our approach is essentially that pioneered by Wagner,[5] except that we ignore possible differences in the diffusivity of various species in the vapor phase.

Consider inserting a piece of Si into a furnace which contains some molecular oxygen. Two oxidation reactions are possible:

$$2Si + O_2 \rightarrow 2SiO(g) \quad \text{active oxidation} \quad (21a)$$

$$Si + O_2 \rightarrow SiO_2(l) \quad \text{passive oxidation} \quad (18)$$

The volatility diagram is useful in differentiating active and passive oxidation and defining the active-passive transition. Figure 16(A) shows a schematic view of the active oxidation process. Oxygen molecules diffuse through a stagnant layer at the gas/solid interface and react with Si to form SiO molecules, which then diffuse away from this interfacial layer into the ambient. According to the

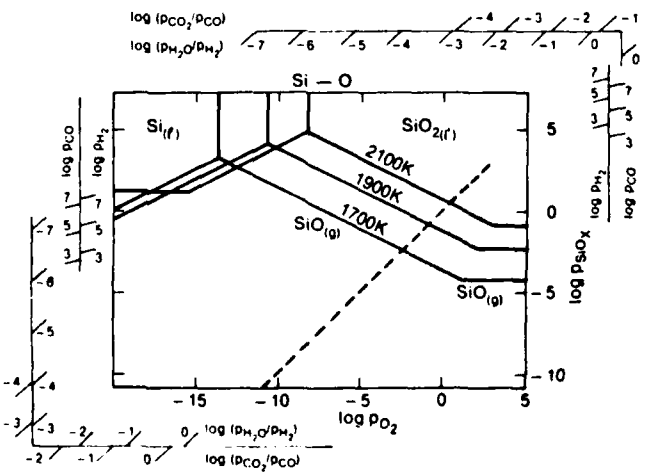

Fig. 14. Complete volatility diagram for the Si-O system.

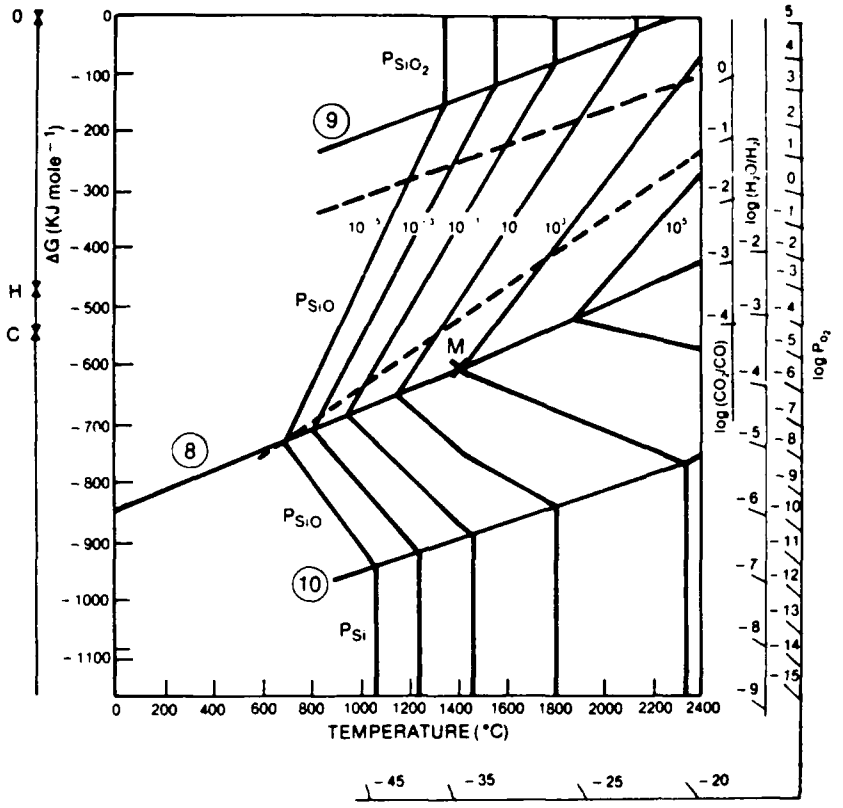

Fig. 15. Ellingham-type diagram for the Si-O system.

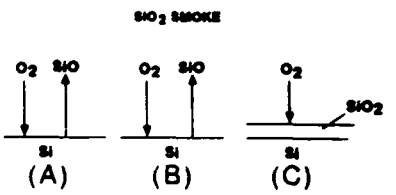

Fig. 16. Schematic view of active and passive oxidation of silicon; see text for discussion.

JANAF Tables, the equilibrium constant for Eq. (21*a*) at 1700 K is $\approx 10^{16}$. Thus, one can make the assumption that all the oxygen molecules arriving at this interface from the ambient are converted into SiO(*g*). Based on this and the assumption that oxygen molecules arrive and SiO molecules depart at the same rate, active oxidation involves the generation of two SiO molecules for each oxygen molecule arriving at the Si surface. Therefore, at the interface $p_{SiO} = 2p_{O_2}$ in the ambient. (This condition is in fact the same as for the isomolar line.) For example, at 1700 K, if the ambient p_{O_2} is 10^{-15} Pa, then the p_{SiO} generated at the interface is 2×10^{-15} Pa. According to Fig. 17, this is many orders of magnitude lower than the equilibrium p_{SiO} — $\approx 10^3$ Pa (point *a*) — and hence SiO(*g*) should not condense. If the p_{O_2} is increased, the p_{SiO} will increase accordingly; at $p_{O_2} = 10^{-12}$ Pa (point *b*) for example, the system should be in the SiO_2 phase field; however, active oxidation will continue because the p_{SiO} is still far below the critical condensation value of $\approx 10^3$ Pa at this point. As the p_{O_2} is further increased, p_{SiO} approaches the critical value and SiO_2 smoke can form away from the interface (Fig. 16(*B*)). This active → active + smoke transition in fact occurs at the isomolar point (*c*). If p_{O_2} is further increased to 5×10^2 Pa, p_{SiO} is 10^3 Pa. This latter pressure will have exceeded the maximum equilibrium pressure defined by point *T*, and SiO_2 will begin to condense on the silicon surface. Beyond this point, a passive SiO_2 film will form, log p_{SiO} will drop from 10^3 Pa at point *T* to 10^{-4} Pa (point *d*), and weight loss will effectively cease. This is passive oxidation and is shown schematically in Fig. 16(*C*). *The active-passive transition, although defined in terms of* p_{O_2}, *is determined by SiO vapor pressure:* p_{O_2} *at the active-passive transition* = $\frac{1}{2}p_{SiO}$ *at point T.*

One can put forward similar arguments for a hydrogen environment. Unlike the previous case, however, the oxygen carrier is H_2O. Two oxidation reactions are possible:

$$Si + H_2O \rightarrow SiO(g) + H_2 \quad \text{active oxidation} \quad (26)$$

$$Si + 2H_2O \rightarrow SiO_2(l) + 2H_2 \quad \text{passive oxidation} \quad (27)$$

The method of construction of the H_2O/H_2 nomograph enables the direct determination of the corresponding p_{O_2}. For example, at point *b* in Fig. 17, log $p_{O_2} = -12$ (Pa) and the corresponding H_2O to H_2 ratio is 10^{-4}, as is determined by noting the intersection on the H_2O/H_2 scale of a line through point *b*. One can assume, as in the previous case, that all the H_2O molecules are consumed by reaction (26) to form SiO(*g*) and a simple relation — p_{SiO} at the interface = p_{H_2O} in the ambient — is maintained. (This in fact is the condition for the isobaric lines.) Inserting a piece of Si into a furnace containing H_2O/H_2 at a ratio of 10^{-4} at $p_{H_2} = 10^5$ Pa will generate 10 Pa of SiO(*g*), and as this is below the critical condensation value of $p_{SiO} = 10^3$ Pa at point *T*, active oxidation will occur. With increasing H_2O to H_2 ratios, SiO_2 smoke will form when the ratio exceeds 10^{-3} (the condition at the isobaric point *e* on Fig. 17); the active-passive transition occurs when the ratio is 10^{-2}, as the SiO pressure at the triple point is then realized. At this condition, p_{SiO} will drop from 10^3 Pa (point *T*) to 1 Pa; this pressure (point *f* on Fig. 17) is determined by the intersection of the 10^{-2} point on the H_2O/H_2 scale with the maximum equilibrium pressure line. The difference between molecular O_2 and H_2O/H_2, $T \rightarrow d$ and $T \rightarrow f$, respectively, is caused only by the thermodynamics of the H_2O/H_2 equilibrium. In the latter case, the active-passive transition occurs when p_{H_2O} in the ambient = p_{SiO} at point *T* and the system must change to point *f*.

IV. Summary and Conclusions

Volatilization reactions in a metal-oxygen system in nonreactive or reducing environments can be fully understood using either volatility diagrams or Ellingham-type diagrams. Three pairs of such diagrams are shown in this paper, Figs. 6 and 7 for the Mg-O system, Figs. 10 and 11 for the Al-O system, and Figs. 14 and 15 for the Si-O system. The construction of these diagrams is somewhat more involved than the classical Ellingham diagram but is just as simple from an application viewpoint. Use does, however, require some understanding of the significance of the *isomolar lines*

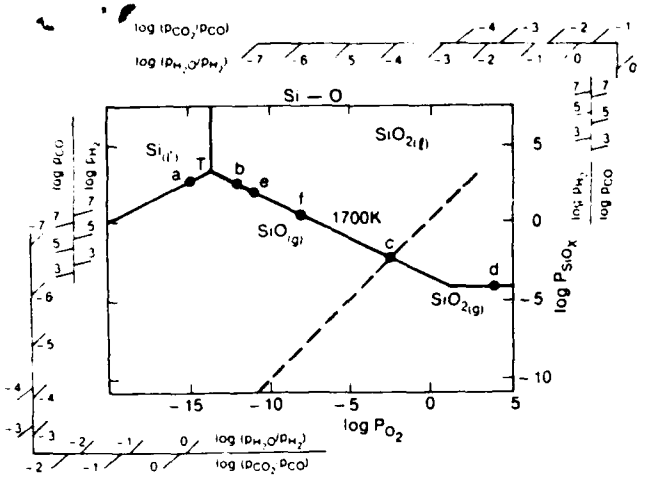

Fig. 17. Volatility diagram for the Si-O system at 1700 K. Points *a–f* refer to discussion in text on active and passive oxidation of Si.

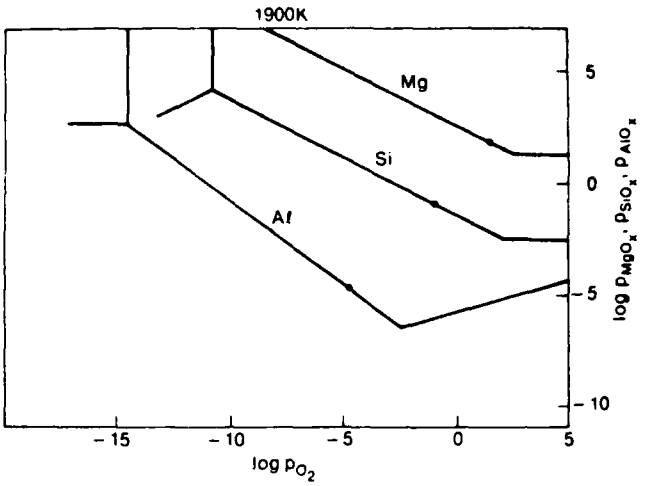

Fig. 18. Comparison of volatility diagrams for the Mg-O, Al-O, and Si-O systems at 1900 K.

in neutral ambients and the *isobaric lines* in reducing ambients, in order to identify the valid portions of the diagrams — in fact, these *iso* lines are the principal original contributions of this paper.

The question of the relative merit of the volatility diagrams vs the Ellingham-type diagrams is interesting. On the one hand, the latter is more widely used in general, because of the convenient representation of the data, but volatility diagrams are popular with high-temperature scientists interested in gas-solid reactions because the species of interest, MO, gas, is plotted as one of the axes. Secondly, their use makes it easier to decide which vapor species in gas-solid reactions are important and to delineate valid *regions of the* p_{O_2}-p_{MO_x} fields, and in this way are a useful intermediate step in constructing an Ellingham-type diagram. Thirdly, they are much more useful than Ellingham-type diagrams when dealing with solid solutions, oxycarbides, and oxynitrides, as will be discussed in future papers. Fourthly, it is a simple matter to compare the volatility of different oxides at a single temperature by noting the p_M or p_{MO}, where the isomolar line intersects the maximum equilibrium pressure line (Fig. 18). Thus, it is easy to see that Al_2O_3 is the least volatile and MgO the most volatile of the three oxides considered, in accord with common laboratory experience; furthermore, it is easy to see why all three of the oxides under consideration cannot easily be reduced to their elements — in all cases, access to the conditions where metal, solid or liquid oxide, and gaseous species can coexist requires very high pressures of reducing gases.

Finally, it is convenient to use volatility diagrams to determine the transition from active to passive oxidation, which occurs in those systems where a volatile MO_2 species predominates, as in the Si-O system.

APPENDIX

The constant dew point lines can be shown to plot as straight lines in volatility diagrams using the following derivation. The important reactions here are

$$MgO(c) \rightarrow Mg(g) + \tfrac{1}{2}O_2(g) \qquad (A\text{–}1)$$

and

$$H_2 + \tfrac{1}{2}O_2 \rightarrow H_2O(g) \qquad (A\text{–}2)$$

The equilibrium constants for these reactions can be expressed in terms of the partial pressures as well as the entropies and enthalpies of these reactions:

$$\log K_1 = \log \frac{p_{Mg}p_{O_2}^{1/2}}{a_{MgO}} = -\frac{\Delta H_1}{2.3RT} + \frac{\Delta S_1}{2.3R} \qquad (A\text{–}3)$$

$$\log K_2 = \frac{p_{H_2O}}{p_{H_2}p_{O_2}^{1/2}} = -\frac{\Delta H_2}{2.3RT} + \frac{\Delta S_2}{2.3R} \qquad (A\text{–}4)$$

By rearranging Eqs. (A–3) and (A–4) one can eliminate T, and by assuming a_{MgO} to be unity, we find

$$\frac{1}{\Delta H_2}\left[\frac{\Delta S_2}{2.3R} - \log \frac{p_{H_2O}}{p_{H_2}p_{O_2}^{1/2}}\right] = \frac{1}{\Delta H_1}\left[\frac{\Delta S_1}{2.3R} - \log (p_{O_2}^{1/2}p_{Mg})\right]$$

which can be simplified to the temperature-independent form

$$A \log p_{Mg} + B \log p_{O_2} + C \log \frac{p_{H_2O}}{p_{H_2}} + D = 0 \qquad (A\text{–}5)$$

where

$$A = 1/\Delta H_1$$

$$B = \tfrac{1}{2}[(1/\Delta H_1) + (1/\Delta H_2)]$$

$$C = -(1/\Delta H_2)$$

$$D = (1/2.3R)[(\Delta S_2/\Delta H_2) - (\Delta S_1/\Delta H_1)]$$

According to this equation, at constant H_2O/H_2, log p_{Mg} decreases linearly with log p_{O_2}.

Similarly the relation between log p_{O_2} and log p_{Mg} (or log p_{H_2O}) as depicted by the isobaric lines will be derived here. The two important reactions are water formation and magnesia reduction by hydrogen.

$$H_2 + \tfrac{1}{2}O_2 \rightarrow H_2O(g) \qquad (A\text{–}6)$$

$$MgO(c) + H_2 \rightarrow Mg(g) + H_2O(g) \qquad (A\text{–}7)$$

The equilibrium constants are

$$\log K_6 = \log \frac{p_{H_2O}}{p_{H_2}p_{O_2}^{1/2}} = -\frac{\Delta H_6}{2.3RT} + \frac{\Delta S_6}{2.3R} \qquad (A\text{–}8)$$

$$\log K_7 = \log \frac{p_{Mg}p_{H_2O}}{a_{MgO}p_{H_2}} = -\frac{\Delta H_7}{2.3RT} + \frac{\Delta S_7}{2.3R} \qquad (A\text{–}9)$$

But $p_{Mg} = p_{H_2O}$ according to the mass balance criterion and by assuming $a_{MgO} = 1$, Eq. (A–9) becomes

$$\log K_7 = \log \frac{p_{Mg}^2}{p_{H_2}} = -\frac{\Delta H_7}{2.3RT} + \frac{\Delta S_7}{2.3R} \qquad (A\text{–}9a)$$

By rearranging Eqs. (A–8) and (A–9*a*) and eliminating T, one can again derive an expression which is independent of temperature

$$A \log p_{O_2} + B \log p_{Mg} + C \log p_{H_2} + D = 0 \qquad (A\text{–}10)$$

where

$$A = 1/2\Delta H_6$$

$$B = (1/\Delta H_6) + (2/\Delta H_7)$$

$$C = -(1/\Delta H_7) + (1/\Delta H_6)$$

$$D = (1/2.3R)(S_6/\Delta H_6) - (S_7/\Delta H_7)$$

According to Eq. (A-10), at constant p_{H_2}, log p_{Mg} decreases linearly with log p_{O_2}.

Acknowledgments: Victor L. K. Lou thanks several colleagues at CR&D, General Electric Company, for useful discussions. Professor John Halloran has provided many critical comments. A. H. Heuer acknowledges the Alexander Von Humboldt Foundation for a Senior Scientist Award, which made possible his sabbatical leave at the Max Planck Institut für Metallforschung, Stuttgart, FRG, where the first complete draft of this paper was prepared.

References

[1]O. Kubaschewski and C. B. Alcock, Metallurgical Thermochemistry, 5th ed. Pergamon Press, Oxford and New York, 1977.
[2]Metals Handbook, American Society for Metals, 1948.
[3]JANAF Thermochemical Tables, 2nd ed. National Bureau of Standards, 1971 (Suppl. 1974 and 1975).
[4]I. Barin, Thermochemical Properties of Inorganic Substances. Springer-Verlag, Berlin and New York, 1973.
[5]C. Wagner, "Passivity During the Oxidation of Silicon at Elevated Temperatures," *J. Appl. Phys.*, **29**, 1295 (1958).
[6]K. Blegen, "Equilibria and Kinetics in the Systems Si-N and Si-N-O," *Spec. Ceram.*, **6**, 223 (1974).
[7]I. Colguhoun, S. Wild, P. Grieveson, and K. H. Jack, "Thermodynamics of the Silicon-Nitrogen-Oxygen System," *Spec. Ceram.*, **6**, 207 (1974).
[8]E. A. Gulbransen and S. A. Jansson, "The High-Temperature Oxidation, Reduction and Volatilization Reactions of Silicon and Silicon Carbide," *Oxid. Met.*, **4** [3] 181 (1972).
[9]S. A. Jansson and E. A. Gulbransen, "Thermochemical Considerations of High Temperature Gas-Solid Reactions"; in High Temperature Gas Metal Reactions in Mixed Environments. Edited by S. A. Jansson and Z. A. Foroulis. Metallurgical Society of AIME, New York, 1973.
[10]S. C. Singhal, "Thermodynamics and Kinetics of Oxidation of Hot-Pressed Silicon Nitride," *J. Mater. Sci.*, **11**, 500 (1976).
[11]G. Ericksson, "Thermodynamic Studies of High Temperature Equilibria XII," *Chem. Scr.*, **8**, 100–103 (1975).

Accession For
NTIS GRA&I
DTIC TAB
Unannounced
Justification
By
Distribution/
Availability Codes
Dist | Avail and/or Special
A-1 21

AIR FORCE OFFICE OF SCIENTIFIC